Sensors & Actuators: A. Physical 359 (2023) 114473

Contents lists available at ScienceDirect

Sensors and Actuators: A. Physical

journal homepage: www.journals.elsevier.com/sensors-and-actuators-a-physical

FBG-based sensing system to improve tactile sensitivity of robotic manipulators working in unstructured environments

Vitorino Biazi-Neto [a,b,*], Carlos A.F. Marques [b], Anselmo Frizera-Neto [a], Arnaldo G. Leal-Junior [a]

[a] Graduate Program in Electrical Engineering, Federal University of Espírito Santo, 29075–910 Vitória, ES, Brazil
[b] i3N & Physics Department, University of Aveiro, 3810–193 Aveiro, Portugal

ARTICLE INFO

Keywords:
Optical fiber sensors
FBG
Robotic manipulators

ABSTRACT

The emergence of Industry 4.0 has brought new concepts to the factories that optimize and improve conventional processes. These technologies have brought assignments to the industrial robots that allow them to perform tasks faster and more precisely. The improvement of the robot's proprioception capacity and tactile sensitivity using sensors is a useful approach to achieve those goals. Optical fibers are a viable technology to be used as sensors in robotic devices because they are electrically passive and present electromagnetic immunity. This paper proposes a Fiber Bragg Grating (FBG) based sensing system to monitor robotic manipulators during their operation. It corresponds to smart textiles installed on the robot's body to detect interactions with the environment. A mathematical model is proposed to find what should be the greatest distance between adjacent FBGs to detect contact at any point between them. From this, it is possible to obtain a minimum number of sensors to detect contact at any point and guarantee the highest spatial resolution of the system with lower costs. The tactile system is formed of a group of optical fibers with multiplexed FBGs embedded in silicone rubber. The optical fibers with the sensors are positioned between layers of polyethylene foam and cotton fabric. After the manufacturing process, temperature and force characterization were done on the sensors which make up the smart textiles. In the characterization results, almost all the FBG presented values of R^2 on the linear regression superior to 0.94. Individual analysis is performed for the sensors which present a low coefficient of determination. Finally, the system was tested in an experimental validation in which the robot was hit while executing a task. From the results, it can be observed that the system can provide the position on the robot's body, the amplitude in terms of force and the instant of time in which an external impact occurred.

1. Introduction

The three Industrial Revolutions took place between the 18th and 20th centuries and can be considered historic landmarks for humanity as they were the main consequence for the transition from a rural and feudal to an industrial and capitalist society [1]. During this period, due to the emergence of a set of technologies in the areas of mechanics, electrical and computing, it was possible to improve the manufacturing processes of the industries in terms of productivity, efficiency, and quality of the products [2]. As a result of the technological advances focused on continuous evolution, the so-called Industry 4.0 consists of the fourth stage of industrialization and represents what is most modern in terms of manufacturing processes today. This phase has as one of its main characteristics the use of intelligent devices, equipped with sensors, microprocessors and complete embedded systems that enable a real-time connection of physical and digital systems [3] and enable a productive flow to be obtained fully optimized, integrated, and automated [4].

Unlike Computer Integrated Manufacturing (CIM), in which the production process is completely controlled by computers and does not require human participation, the arrival of Industry 4.0 introduced a change in manipulators operation from an isolated performance from the human collaborator for a cooperative human-robot approach in many situations. This strategy guarantees an improvement of the use of resources and productivity by combining the characteristics of robots with the flexibility and dexterity of humans in dealing with unexpected and non-repetitive tasks. Thus, the workspace in industrial environments has been rethought in organizational terms in order to ensure the protection of human employees who interact with robots [5].

The application of robots in the medical and healthcare fields is

* Corresponding author at: i3N & Physics Department, University of Aveiro, 3810–193 Aveiro, Portugal.
E-mail addresses: vitorino_biazi@hotmail.com, vitorino.biazi@ua.pt (V. Biazi-Neto).

https://doi.org/10.1016/j.sna.2023.114473
Received 9 February 2023; Received in revised form 26 May 2023; Accepted 4 June 2023
Available online 7 June 2023

another case that involves direct interactions between humans and robots, and it has become increasingly common to make medical procedures more reliable and safer [6]. Robotic systems enable more intense treatment, greater repeatability and reduce the therapists' workload when applied in rehabilitation processes [7]. In terms of surgical procedures, many benefits were obtained with the participation of robots, as they compensate for the limitations of dexterity and precision of humans in the manipulation of micro-instruments. In addition, surgeon's exposure to ionizing radiation and physical exhaustion during very long procedures can be reduced [8]. Finally, socially assistive robotics (SAR) is another robot-based strategy to motivate social and cognitive therapy through human-robot interaction [9].

For the presented reasons, research involving more sensitive, accurate and reduced size sensors has become relevant to amplify the proprioception and tactile sensitivity of robots to improve their ability to perceive their own shape and detect external stimuli in an unstructured environment [10]. Thus, it is possible to reach intelligent systems that can sense, interpret, and react to stimuli quickly and efficiently [5] and to ensure a safer working environment.

Technological advances in the late 20th century made it possible to manufacture new types of optical sources, amplification systems and modulation techniques that made the optical fibers a revolutionary tool for telecommunication systems [11]. Besides their traditional use, optical fibers have become a consolidated technology for a series of sensing applications such as healthcare monitoring [12], environmental changes detection in industries [13] and structural and spacecraft health monitoring [14]. One of the main reasons for them being widely used in the sensing field is their intrinsic characteristics such as low weight, compactness, and chemical stability. Additionally, they are immune to electromagnetic fields which can appear when the electrical actuators are activated and distort the results from the conventional electronic-based sensors [15]. The ease of installation of the optical fiber sensors in the structure of already assembled equipment without removing or changing components makes them advantageous in relation to other types commonly used in the instrumentation market. This technology has a substantial growth due to its characteristics and the diversity of parameters that can be monitored such as temperature, force, acceleration, liquid level, humidity, pressure, among others [16].

The Fiber Bragg Grating (FBG) sensors are a type of optical fiber sensor whose intrinsic characteristics are beneficial for the instrumentation of industrial robots. Its high sensitivity to strain and multiplexing capability, which consists of recording several sensors on a single fiber [17], makes it possible to detect soft external stimuli and to use a reduced number of fibers to cover the robot's body with sensors. Therefore, reducing the number of cables installed in industrial equipment is a positive strategy, mainly in terms of cost reduction and better use of workspace [18]. Another important type of application of these sensors are smart textiles, a wearable sensor technology that is commonly applied to monitoring the user parameters. When used by humans, it is relevant to monitor health-related aspects such as kinematics and dynamics of the gait, body temperature and heart and respiration rate. This type of technology also plays an important role in quantifying interactions with the environment, such as detecting forces between users and objects [19]. In [20], the researchers proposed a force sensing robot finger using embedded FBG-based sensors to compensate the effects of deformation on the robot's joints which appears during execution of heavy tasks and consequently improve the quality and precision of the results. In the medical field, minimally invasive surgery (MIS) supported by robotic devices has the disadvantage of eliminating force feedback information and this tactile sensitivity in the surgical tool can be recovered with the aid of sensors. The robotic manipulator for MIS tests proposed in [21] is equipped with FBG sensors on the surgery tool to measure the interaction forces during the process. The FBG independence of source optical power fluctuations and immunity to connection losses were relevant factors for the choice of this type of sensor. The work of [22] proposed to develop an instrumented tool to measure grasping and axial interactions on the surgical process which are commonly hard to monitor. It was possible to achieve good repeatability and to avoid the cross-sensitivity effect of the two interest parameters using the proposed tool.

In another robotic surgery application, a 3D force sensor for microforceps used in robotic-assisted vitreoretinal surgery was proposed using FBG as basis technology [23]. The sensor has the capacity to measure not only the transverse forces but also the force on the tool axis. Lateral FBGs were glued around the tool guide tube using epoxy adhesive to measure the transverse force on the tool tip and a fourth FBG sensor is used to detect forces along the tool axis that appear due to manipulation of the retina.

This paper aims to develop an FBG-based tactile monitoring system for robotic manipulators. A multiplexed system of FBG sensors in smart textiles is installed in the robot body to detect stimuli and robot-environment and human-robot interactions during the execution of collaborative tasks. To test the system, mechanical perturbations were randomly applied to the sensors on the robot's body while it performs the task of transporting an object. The response of the FBGs to the stimuli is then collected by means of an optical interrogator and processed to estimate the intensity and the region of the robot's body where the contact occurred. This guarantees the robot a greater capacity for proprioception and adaptation in unstructured environments to carry out its tasks efficiently.

The paper is divided as follows. Section 2 presents the materials and the techniques used in the development of the sensor system. The system and equipment in which the sensors were tested, the constructive characteristics of the system as well as the tests for validation of the systems after manufacturing are presented and detailed. Section 3 presents the results of the proposed characterization and validation experiments of the tactile system. General discussions about the behavior of sensors are also raised and other relevant points are also highlighted. Finally, Section 4 concludes the paper by presenting its most relevant contributions.

2. Materials and methods

2.1. Test equipment presentation

The practical implementation of the proposed tactile system is made seeking to monitor interactions of the robotic manipulator Kuka KR3 R540 (KUKA Industrial Robots, Germany) with the environment and objects. The robot is an industrial open kinematic chain manipulator formed by mechanical and electrical components. It has 6 Degrees of Freedom (DoF) on its joints and its structural parts are made of cast light alloy. The electrical components include the energy supply systems and all the motors which are used to execute the joint's angular movement. The robot has a mass of 26.5 kg, workspace volume equal to 0.61 m^3 , and maximum reach of 541 mm. One of the robot accessories is the 2-finger electric gripper LEHZ20 (SMC, Japan) for the manipulation and transport of objects. The gripper operates with the drive of its servo motor which causes the approximation of the two parallel surfaces on its inner part and the desired object is then gripped. Fig. 1 presents the robot Kuka KR3 and the gripper LEHZ20.

2.2. Mathematical model to estimate the distance between sensors

For the tactile contact detection system, it is proposed to use a set of optical fibers positioned circularly around the robot's links. In each fiber, a series of FBGs multiplexed is installed so that each sensor covers a part of the link where the optical fiber is positioned. The interactions between the environment and the robot tend to act on the optical fibers as transverse loads.

To achieve a system capable of detecting mechanical touches in many points on the surface of the robot's body, it is necessary to determine the minimal distance between the FBGs and consequently the

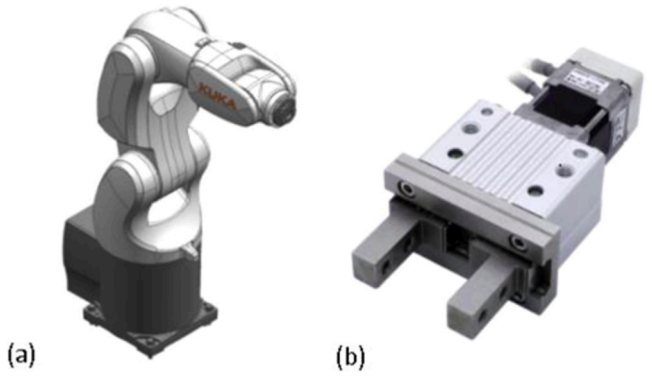

Fig. 1. (a) Robo Kuka KR3 R540 and (b) Electric gripper LEHZ20.

number of FBGs for each link from the geometric characteristics and properties of the materials which makes up the sensing system. The optical fibers from the sensing system undergo a bend when an external stimulus is applied transversely to its axis due to the existence of the substrate between it and the robot body. A reasonable model to consider this is the simply supported beam model with a concentrated load applied at a generic distance x from the first support. Fig. 2 shows the main parameters that are important to solve the model.

L is the length of the optical fiber, P is the interaction/contact force and V_a and V_b are the reactions in the supports. The definition that the sum of forces and moments at a point on a static rigid body are equal to zero is used to obtain the supports' reactions.

The curvature of the fiber due to the interaction with the environment causes the appearance of internal bending moments that vary along the fiber longitudinal axis. The presence of these internal moments results in strains on fiber longitudinal direction that cause wavelength shifts on the FBGs used on the tactile system. For the configuration of Fig. 2, the internal moment along the fiber length may be defined by Eq. (1).

$$M(a) = \begin{cases} -\frac{P\cdot x\cdot a}{L} + P\cdot a, 0 < a < x \\ -\frac{P\cdot x\cdot a}{L} + P\cdot x, x < a < L \end{cases}. \tag{1}$$

It can be guaranteed that the system detects a contact when the FBG closest to the load presents a shift in its central wavelength. This consideration is feasible because this FBG is under the highest values of stress due to bending. Assuming that all FBGs are on the same distance from each other and being c the distance between two adjacent FBGs, the FBG immediately to the left of the force P is positioned in a distance of $x - \frac{c}{2}$ from the left support and the FBG immediately to the right of the force P is positioned in a distance of $x + \frac{c}{2}$ from the left support. Then, the bending moment on the FBGs immediately to the left and right of the concentrated load is given by the Eqs. (2) and (3), respectively.

$$M_L = \left(\frac{x}{L} - 1\right)\cdot\left(\frac{P\cdot c}{2} - P\cdot x\right), \tag{2}$$

$$M_R = P\cdot x\cdot\left(1 - \frac{x}{L} - \frac{c}{2L}\right). \tag{3}$$

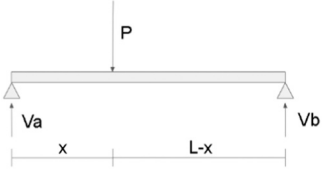

Fig. 2. Parameter of the simply supported beam with a concentrated load.

The maximum fiber deflection is limited by the thickness of the substrate over which it is positioned. For this reason, the fiber suffers small deflections, and its behavior can be modeled by applying the elasticity theory. Considering that the material properties are isotropic, and the material has linear elastic behavior, the bending stresses on the fiber are related to the bending strains by Hooke's Law. Knowing that the optical fiber cross-section is circular, the longitudinal strain at the point farthest from the neutral line as a function of the internal bending moment is presented in Eq. (5).

$$\varepsilon = \frac{32\cdot M}{\pi\cdot E\cdot d^3}, \tag{5}$$

where ε is the bending normal longitudinal strain, $E$is the Young's Modulus of the optical fiber and $d$is the diameter of the optical fiber. Due to the symmetry in the fiber and for simplification purposes, it was decided that only the analyses for the FBG on the left side of the load are sufficient. Ensuring that the minimum resolution of an FBG is achieved for the condition in which the FBG immediately to the left of the load has the lowest deformation values, then the other conditions will also reach. As the longitudinal strain equations are parabolic, the smallest strains are in the FBGs on the fiber ends. Considering the first FBG positioned at $\frac{c}{4}$ of the fiber left end, the maximum strain value on it is given by Eq. (6).

$$\varepsilon_{\min} = \frac{8\cdot P\cdot L\cdot c - 6\cdot P\cdot c^2}{\pi\cdot E\cdot d^3\cdot L}. \tag{6}$$

The value of the concentrated load at a distance x from the left support of a simply supported beam that can be applied to achieve the maximum deflection of the fiber is given by Eq. (7).

$$P = \frac{\pi\cdot e_{\max}\cdot E\cdot d^4\cdot L}{8\cdot\left(L\cdot c - \frac{3\cdot c^2}{4}\right)\cdot\left(L^2 - \frac{9\cdot c^2}{16} - \left(L - \frac{3\cdot c}{4}\right)^2\right)}. \tag{7}$$

where $e_{\max}$is the maximum deflection on the fiber for the analysed condition. When this force value is reached, the fiber begins to undergo a transverse deformation (as shown in Fig. 3) that affects the longitudinal deformation of the fiber by Poisson's effect.

F is the force per unit length, $2b$ is the contact width, U is the diametric compression and R is the radius of the cylinder. The work from [24] provides some models to calculate the cross-section deformation of a cylinder compressed between two flat plates. Extending the approach to the optical fiber, the half contact width is obtained from Eq. (8). The model from [25] was chosen for the relative displacement between two flat plates (Eq. 9).

$$b = \sqrt{\frac{2\cdot F\cdot d}{\pi}\cdot\left(\frac{1}{E_t} - \frac{\nu^2}{E}\right)}, \tag{8}$$

$$U = \frac{4\cdot F}{\pi}\cdot\left(\frac{1}{E_t} - \frac{\nu^2}{E}\right)\cdot\left(\ln\left(\frac{d}{b}\right) + \frac{1}{3}\right), \tag{9}$$

$E_t$is the transversal modulus of the optical fiber. The transverse deformation of the fiber also has an effect of longitudinal deformation on the fiber length. Eq. (10) provides the strain on the FBG on the extremity of the fiber.

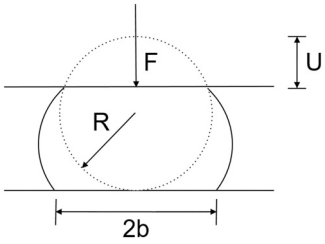

Fig. 3. Representation of the fiber undergoing a transversal deformation.

$$\varepsilon = \varepsilon_{\min} + \nu \cdot \frac{U}{d}, \tag{10}$$

The mechanical properties of the silica fiber were obtained from the works of [26] and [27]. The lower touch sensitivity of the human skin happens in the forehead and in the palm and is equal to 0.7mN [28]. Unlike a human, robotic manipulators have high robustness and inertia and a low magnitude force should be insufficient to compromise their movement. For this reason, it can be assumed that the tactile system does not need a touch resolution as low as human skin.

Assuming that the lower strain detected by the sensors is the strain resolution of a 2 mm length FBG (from the work of [29]), it is possible to obtain the average distance between FBGs from the proposed model. Table 1 presents the geometric characteristics of the optical fiber and the mechanical properties used on the model to evaluate the distance between FBGs in the tactile system.

Considering the data in Table 1, the lowest value of force to detect contact in the fiber and the resolution of the FBGs, it is possible to solve the mathematical modeling equations that provide the strain value on the FBG at the left end of the beam as a function of the distance between the FBGs for the case in which the force is closer to the left support. Fig. 4 presents the strain of the far left FBG for the project critical case as function of the distance between FBGs. The distance between FBGs which provides the strain value almost equal to the resolution of the FBG was also marked in the graph.

The distance obtained from the mathematical model is equal to approximately 60 mm to achieve a system in which it is possible to detect contact along the total length of the fiber. The minimum number of sensors will be one plus the value of the division between its useful fiber length on the robot body and the distance between sensors for contact detection obtained from the mathematical model. Due to the limitations related to the high cost of fabrication of the FBGs and availability of phase masks in the laboratory, it was necessary to reduce the number of sensors obtained from the mathematical model and, consequently, the spatial resolution of the system.

2.3. Constructive characteristics of the tactile system

Fig. 5 presents a scheme of the nomenclature used to refer to the sensors of the tactile system. The links with the textiles were numbered from 1 to 4 starting from the closest to the end effector and the FBGs in each fiber were numbered in ascending order with the first one being the closest to the APC connector. The numbers under the dotted lines represent the distance between the FBGs. The dimensions and positions on the robot's links of each smart textile can also be seen in Fig. 5. The production of the FBGs was accomplished with a pulsed Q-switched Nd: YAG laser system (LOTIS TII LS-2137 U laser), emitting at 266 nm with a pulse repetition rate of 10 Hz and 25 J of pump energy. The inscription setup is based on the phase mask technique, in which the laser beam goes through four mirrors and a plano-convex lens before reaching the phase mask as reported in [30].

It was chosen to position the optical fibers far from the robot's joints, where the deformations are critical, in order to avoid the optical fibers rupture. Therefore, four fibers are needed, one for each link, to cover the regions of the robot's body most exposed to interactions with the environment. The perimeter of the links' cross section was measured so that it was possible to dimension the fibers for each one of them. The link closer to the end effector tends to be more susceptible to external stimuli due to more interaction with the environment and, therefore, is equipped with a greater number of sensors.

Table 1
Optical fiber characteristics for estimating the distance between FBGs.

Characteristics	Silica optical fiber
Young's Modulus (GPa)	70.0
Poisson's ratio	0.17
Fiber diameter (mm)	0.245
Lower force value (mN)	0.7
Fiber length (mm)	600
Strain Resolution (με)	10

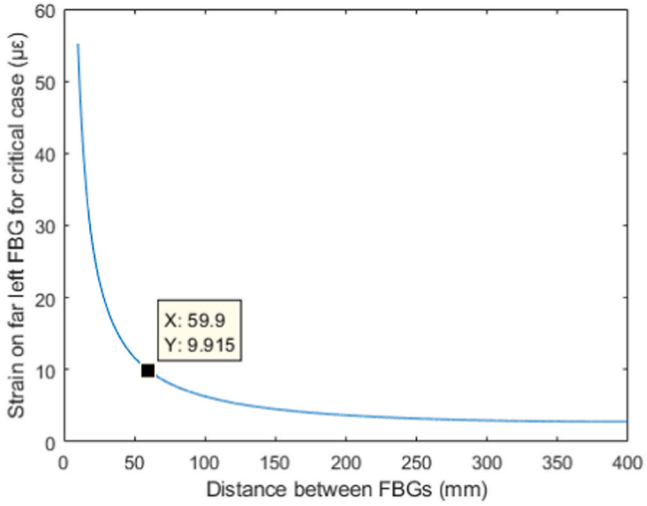

Fig. 4. – Mathematical model solution to estimate the distance of FBGs in detection system design.

To improve the mechanical resistance and robustness of the sensors, the regions of the optical fibers with the FBGs were embedded in a small volume of cured silicone rubber. The sensors were positioned on supports made with the Liquid Crystal Display (LCD) based Stereolithography (SLA) 3D printer Photon (Anycubic, China) and then the liquid silicone rubber mixed with 10% by mass of catalyst was poured into the supports. It waited for 24 h to ensure that the curing process was complete. One end of the fibers has been cleaved and joined to APC connectors so that the reflection spectrum can be monitored with an optical interrogator.

Each one of the smart textiles is formed by an inner layer of two polyethylene foams between which optical fibers are positioned for greater mechanical protection. The polyethylene foams are then sewn between two external layers of cotton fabric. Touch fasteners were glued to the textile ends to be able to attach the sensing system to the robot's body.

2.4. Temperature and force characterization

After the manufacturing process of the smart textiles, tests were carried out for each sensor of the tactile system to obtain their sensitivity to temperature variation and force. The smart textiles were positioned inside the climatic chamber Q315C21N (Quimis, Brazil) and the reflection spectrum of each optical fiber was monitored with the optical interrogator HYPERION si255 (Luna, USA). The temperature selected as a reference to calculate the wavelength shifts of the FBGs was equal to 25 °C. The range of temperature for the tests was from 25 °C to 45 °C with increments of 5 °C. This temperature range was chosen for the characterization of the sensors, as industrial robots operate mainly performing tasks in production and storage lines, in the automotive industry and in the medical area [31,32], where they are not commonly under the effect of high temperatures. Once reached, each temperature was held for 5 min to ensure stability and then the spectra data were saved. A small offset was present in relation to the desired set-points presumably due to the inaccuracy of the climate chamber controller. From the saved data was possible to obtain the curves that correlate the central wavelength shifts of each FBG with temperature variations. Fig. 6 shows the internal construction of the smart textile positioned on the link 1.

For the force characterization, the FBGs of the smart textiles were

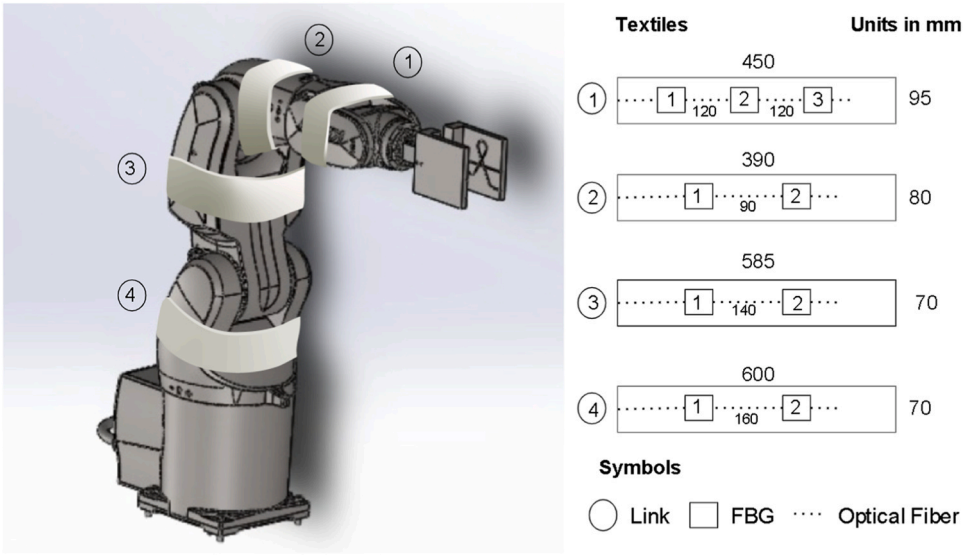

Fig. 5. Nomenclature used for the smart textiles and FBGs installed on the robot's body.

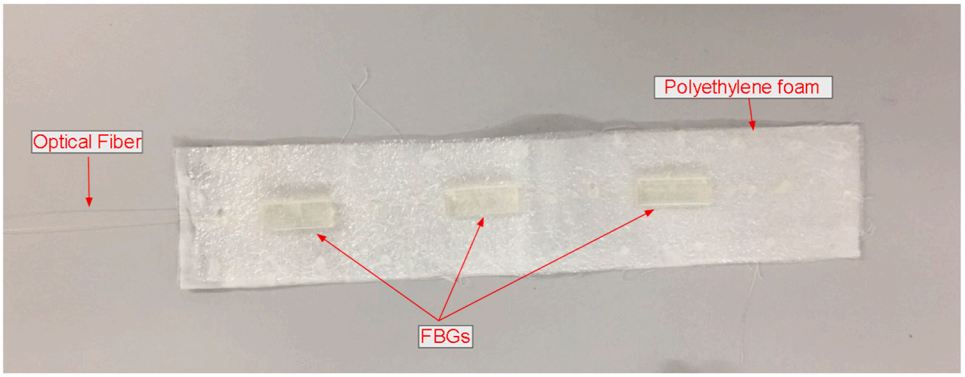

Fig. 6. Internal components that make up the smart textiles.

positioned separately on the Universal Machine (Biopdi, Brazil) base and a compression tool was installed on the machine to apply the compression forces on them. The machine is equipped with a load cell to measure the force values during the experiments. The force values ranged from 0 N to 50 N with increments of 10 N and the reflection spectra of the FBGs were collected with the interrogator HYPERION si255. Due to the relaxation effects that occur in the viscoelastic materials that make up the structure of the sensors, the force values measured in the machine showed a real-time decrease. It was necessary to wait one minute for force stabilization at each measured point. All the force characterization tests were done in an environment with controlled temperature. Fig. 7 presents the universal machine used during the force characterization of the smart textile sensors.

2.5. Experimental validation

To evaluate the performance of the tactile system, a set of experiments was proposed. Each smart textile was circularly fixed to the respective link of the robot using the touch fasteners. Initially, the behavior of the sensors was observed while the manipulator performed a trajectory without external interference and, then, it was compared with the response of the sensors when the robot is hit by a rubber mallet. From the disturbances that appear in the signal of the FBGs, it is possible to know the instant that the impact occurred and the location of the robot's body that was hit. Fig. 8 shows a scheme of the proposed tactile system after installation on the robot.

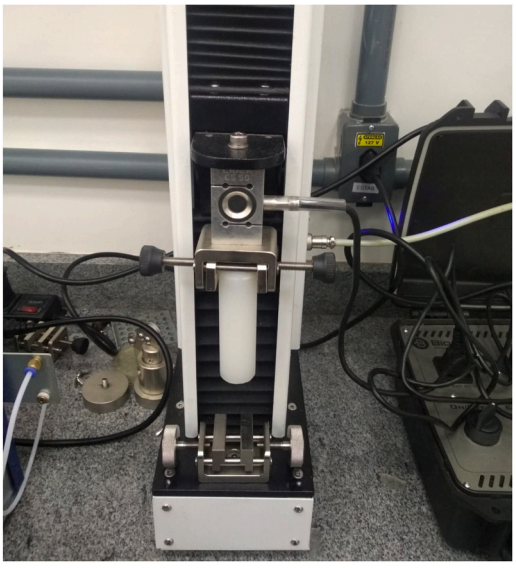

Fig. 7. Universal test machine for the force characterization experiments.

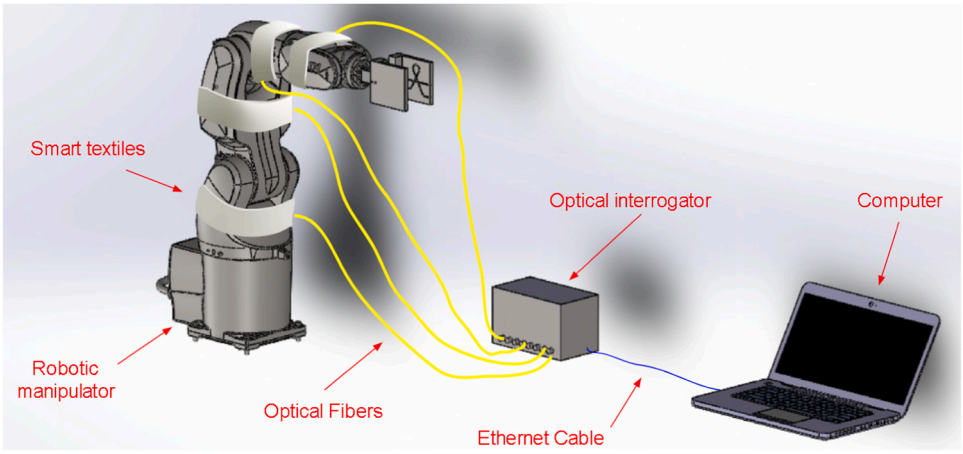

Fig. 8. Tactile sensing system installed on the robot.

The smart textiles were placed on the robot links and the optical fibers were plugged in different channels of the interrogator HYPERION si255. An Ethernet cable is used for communication between the interrogator and a computer for processing the FBGs' data. Since the impacts done with the rubber mallet on the robot body occur in an extremely small-time interval, it is necessary to use a high sampling frequency to avoid loss of relevant data. The trajectory of the robot's during the tests is formed by the movements of approaching a table, returning to the

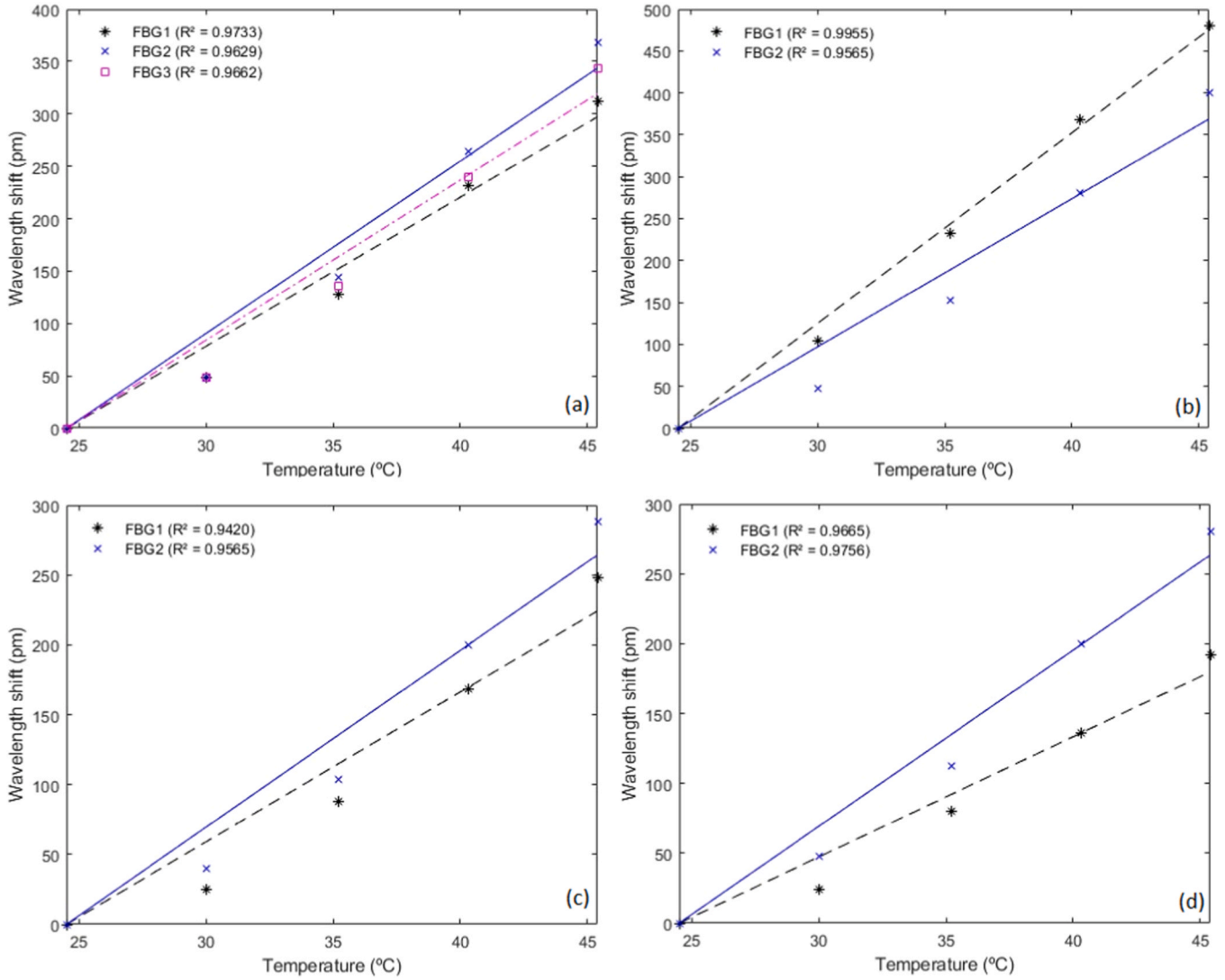

Fig. 9. Temperature characterization of smart textiles in relation to (a) link 1, (b) link 2, (c) link 3 and (d) link 4.

starting position, and finally returning to the table.

Three different tests were executed for validation of the tactile system:

(1) execution of the proposed trajectory without any external interference.
(2) execution of the proposed trajectory with the left side of the robot being hit by the hammer.
(3) execution of the proposed trajectory with the frontal side of the robot being hit by the hammer.

Each test was executed three times with the end effector at a speed of 250 mm/s and the Bragg wavelength of each FBG were saved during the robot's movements with a sampling frequency of 1 kHz. A high sampling frequency value was chosen so that it is possible to detect high frequency components, such as impacts and the effects on sensor response that can arise from high speed robot movements, and try to avoid problems such as aliasing [33]. In each repetition of the three tests, the impacts on the FBGs on the left and front sides of the robot's body were given in random sequences and time instants. Due to the constraints in the sensor manufacturing process, it was impossible to inscribe an adequate quantity of FBGs on the fibers for placement on all four sides of the robot's links. Nevertheless, it is sufficient to validate the system on just one of the parallel faces due to the inherent symmetry in the links. Temperature was controlled at a constant value of 25 °C during the experiments.

3. Results and discussion

3.1. Temperature and force characterization

Fig. 9 shows the linear models fitted from the points collected during the temperature characterization for each FBG in the smart textiles from links 1–4, respectively.

For information obtained from the compression tests, Fig. 10 shows

Table 2
Sensitivities of the tactile system sensors.

Link	Sensor	Temperature sensitivity (pm/°C)	Force sensitivity (pm/N)
Link 1	FBG 1	14.22	9.73
	FBG 2	16.44	6.07
	FBG 3	15.28	3.69
Link 2	FBG 1	22.74	11.41
	FBG 2	17.65	7.97
Link 3	FBG 1	10.73	25.77
	FBG 2	12.65	23.48
Link 4	FBG 1	8.60	1.26
	FBG 2	12.60	27.53

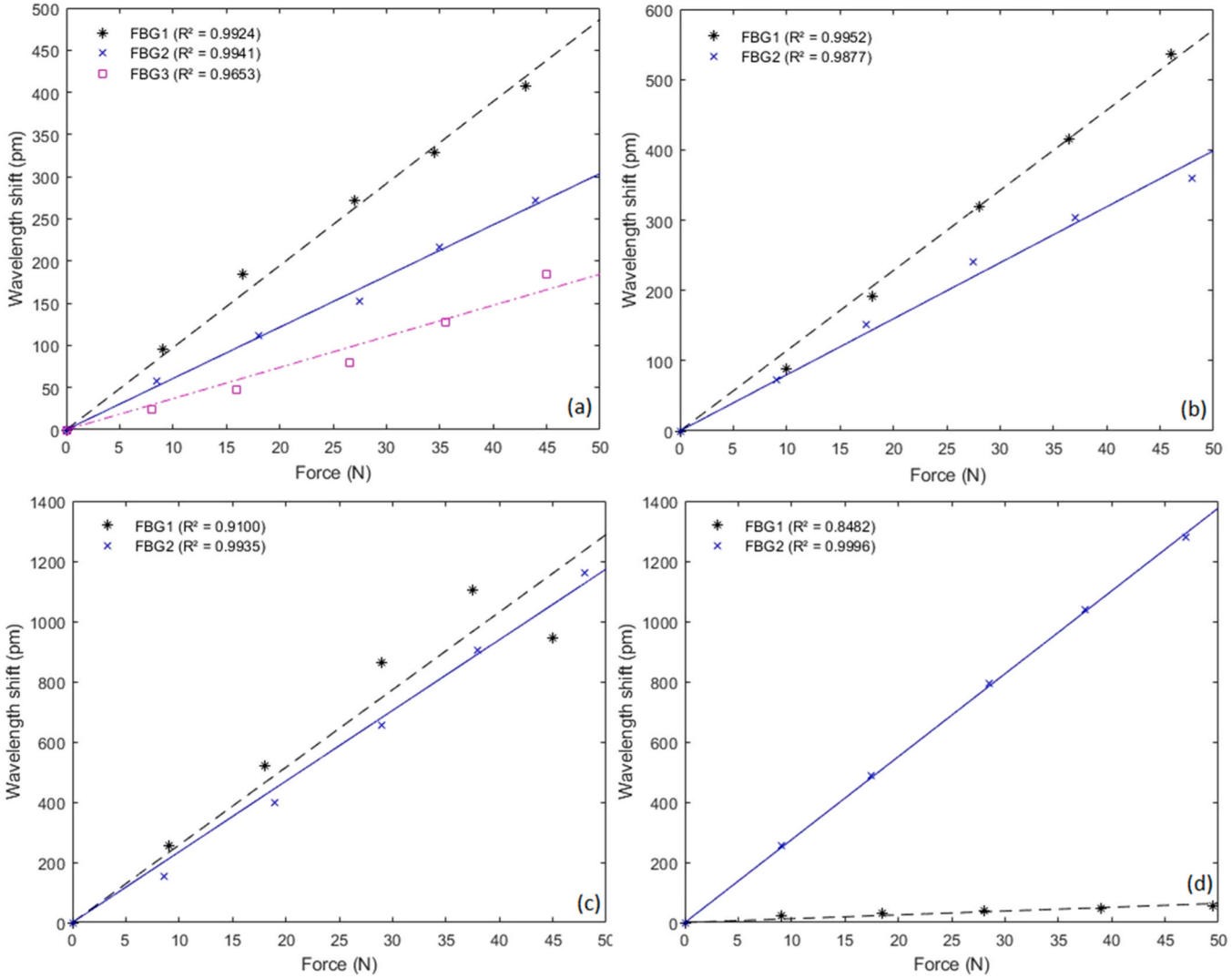

Fig. 10. Force characterization of smart textiles in relation to (a) link 1, (b) link 2, (c) link 3 and (d) link 4.

the characterization of each of the sensors that make up the smart textiles of links 1–4, respectively.

Table 2 presents the sensitivities relative to temperature and force of all sensors according to the convention of Fig. 5.

Temperature characterization is relevant for situations where the robot operates in environments with temperature fluctuations and can work together with temperature compensation strategies to avoid cross-sensitivity with the parameter of interest. However, since a thermal plant exhibits a slow time response, it may be easy to separate the impact response on the sensors from the temperature response by this difference in frequencies. A Fourier analysis can show that the Bragg wavelength shifts related to temperature variations prevail in the low frequency band and the Bragg wavelength shifts related to robot dynamics are in the high-frequency band. From this, a high-pass filter may be designed to eliminate the signal components related to the temperature variation as done in [34].

As the manufacturing process of the sensing system is carried out manually, the sensitivity of the sensors is expected to vary significantly from one to the other as can be seen in Table 2. For the supports of the sensors containing a higher volume of silicone rubber, it is expected a higher thermal expansion of the material which tends to cause greater deformations in the sensors. For this reason, when the volume of silicone in the support is greater, higher temperature sensitivity is expected. In relation to force, a small deformation is obtained for a high volume of material, since the stiffness of the material is greater. Consequently, sensors with more silicone tend to be less force sensitive.

For FBGs in which there is an excess of silicone volume in relation to the available volume of the support, the material that overflows tends to form a convex-shaped surface due to the effect of superficial tension before the cure of the material. Due to the curvature of the surface, it is difficult to ensure that the load is applied perpendicular to the silicone surface. For this reason, in some cases, the force may have been applied obliquely to the upper surface of the support and interfered with the sensitivity value.

Linear regression was used to obtain the relation between temperature variation and force with the central wavelength shift on the FBGs. The linear fitting was chosen for the sensor characterization due to its simple implementation and because it is more conservative when compared to non-linear models. For the linear regression, the presence of outliers in the data can cause a reduction in the accuracy of the fit, however there is less chance of overfitting the model to the data at these points which move the curve away from the expected values in an interval close to the outliers, as tends to occur in the non-linear fit, especially in more complex models [35]. Almost all the lines which are shown in Figs. 9 and 10 have a coefficient of determination R^2 greater than 0.94 which indicates a significantly linear behavior. The R^2 lower than 0.94 of some curves is directly related to outliers on the data. The last point collected for FBG 1 on link 3 presented a smaller wavelength shift than the penultimate point. In this case, the sensor support may have been moving at the base of the machine so that the load was not applied at its center. If the load was applied to a more rigid region, such as the 3D printed support, then the sensor would experience less deformation and, consequently, a smaller wavelength shift. A similar approach can be considered for the high wavelength shift difference between the first and second points of FBG 1 on link 4.

Compared to the other sensors, the lower sensitivity to temperature and force of FBG 1 on link 4 may be related to the volume of silicone rubber positioned on its 3D printed support. It is assumed that the volume of silicone rubber was insufficient to fully embed the sensor and fill the support. The compressive force of the characterization is then applied directly to the support, which is more rigid than the silicone rubber and consequently, the sensitivity of this FBG tends to be lower. The incomplete embedding of this FBG prevents the thermal expansion of the silicone from causing the same level of deformation that occurs in other sensors and consequently, reduces its sensitivity to temperature.

As the FBG-based sensors are embedded in silicone rubber, the viscoelastic characteristics of the polymers, such as creep and relaxation, can result in a hysteresis effect on the sensors, which is a difference in the sensor response when it is under cyclic loading conditions [36]. The use of a viscoelastic modeling approach is suggested to lead with these time-dependent effects [37]. However, since the sensors presented high linearity without viscoelastic compensation and their sensitivity has no direct correlation with hysteresis [38], the previous characterization is sufficient to attend the experimental analysis from this work carried out in very short intervals of time.

3.2. Experimental validation

For analysis of the tactile system, Fig. 11 presents the Bragg wavelength shift of the FBGs on the links 1–4 for one of the tests without external perturbation. The variations were considered in relation to the design Bragg wavelength.

As can be seen in Fig. 11, during the movements without external perturbations the variation of the central wavelength of the FBGs were all inferior to 40 pm except for the FBGs on the link 1 in the interval of 50–55 s. Even with this, it is not possible to assume that the variations were due to the robot's movements as they may be of a noisy nature.

As the FBGs are positioned over the robot's links, it is expected that they behave similarly to a rigid body and do not deform during movement. If an optical fiber was shared by two different links, their FBGs would present a variation in their central wavelength due to the change in the joint angle [39]. This avoids the need for complex signal processing algorithms to separate responses of different sources in the reflection spectrum. The non-abrupt variations in the signal observed between 50 s and 55 s for the FBG 1 on link 3 were due to the textile moving slightly in the links.

Fig. 12 presents the behavior of the FBGs in the links 1–4 for the experiments with the impacts on the left side of the robot's body.

The FBGs 1 of each link were the ones that detected higher wavelength shifts for the tests with impacts on the left side of the robot. The FBGs that are far from the impact region have extremely lower Bragg wavelength shift than those that are closer.

Fig. 13 presents the behavior of the FBGs in the links 1–4 for the experiments with the impacts on the front side of the robot's body. The intensity of the wavelength shift which happens in each sensor is related to the position of the impact and the sensitivity to force of the sensor. For a given impact, if the FBG is hit directly by the hammer and has high force sensitivity, the wavelength shift tends to be greater.

The FBGs 2 of each link were the ones that detected higher wavelength shifts for the tests with impacts on the front side of the robot. Similar to the previous case, the other FBGs adjacent to the impact region in the optical fiber also suffer deformation and consequently a wavelength shift at the moment of the impact. If a collision occurs between two adjacent sensors, it is not possible to determine the exact point which it hit. For this reason, to amplify the spatial resolution of the system, it's necessary to increase the number of FBGs in each optical fiber or to implement a Machine Learning based solution.

For this type of test, it is not possible to compare the FBGs quantitatively in terms of sensitivity to force. This difficulty arises from the fact that the human operator of the rubber mallet has no control over the force that he applies on impact. As an impact can be considered the impulse of a force acting in a very short interval of time, it is possible to measure the effect of the impact on the robot's body in terms of force through the sensors' force characterization from Fig. 10. As a load cell was used as force control equipment in the sensor calibration process, it is expected that equivalent values of force for the impacts are physically correct. Figs. 14 to 16 show the estimated force values relative to the tests of the Figs. 11 to 13.

The wavelength shift tends to be small for FBGs further away from the impact site. In this case, it is possible to identify the impacts and the moments they occur from at least one of the peaks data from an optical fiber detected by the interrogator. This approach was used for link 2 as

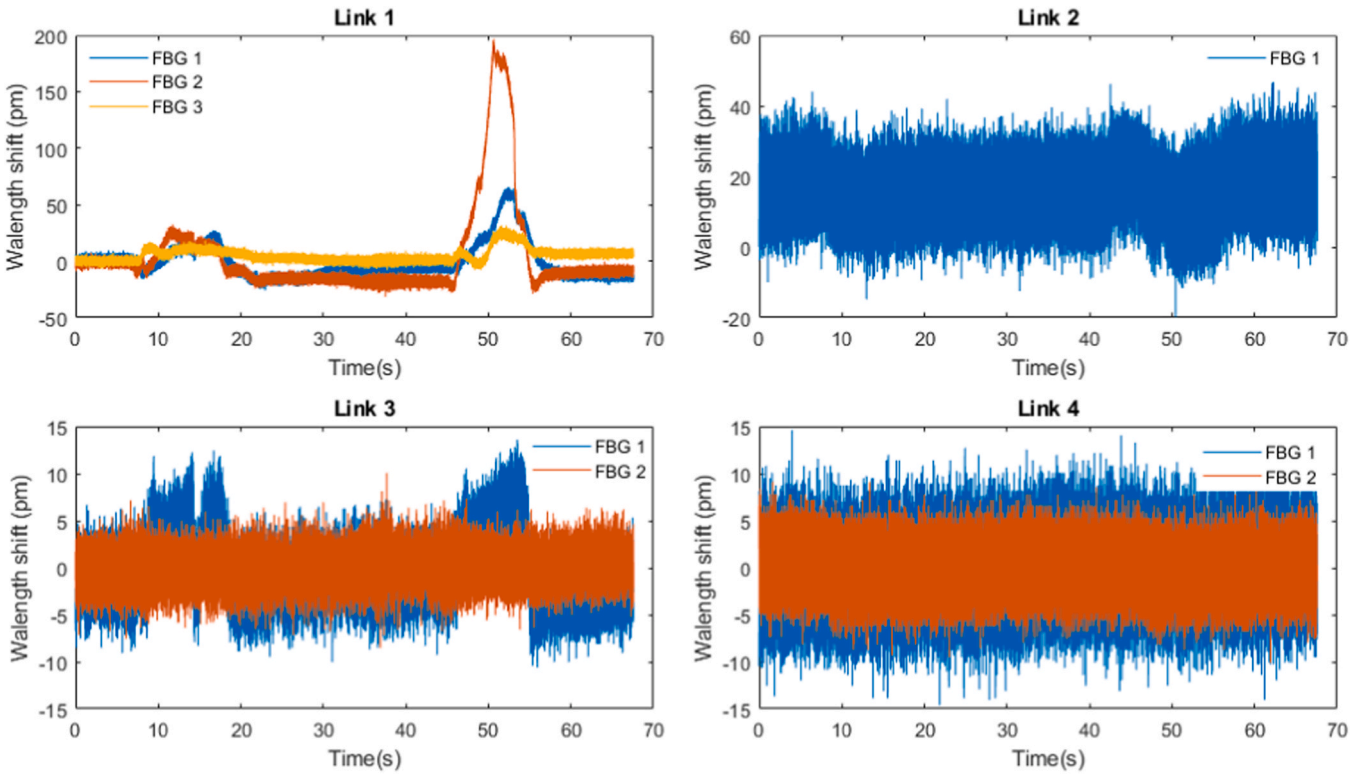

Fig. 11. Sensors response during the test of the tactile system without external perturbations.

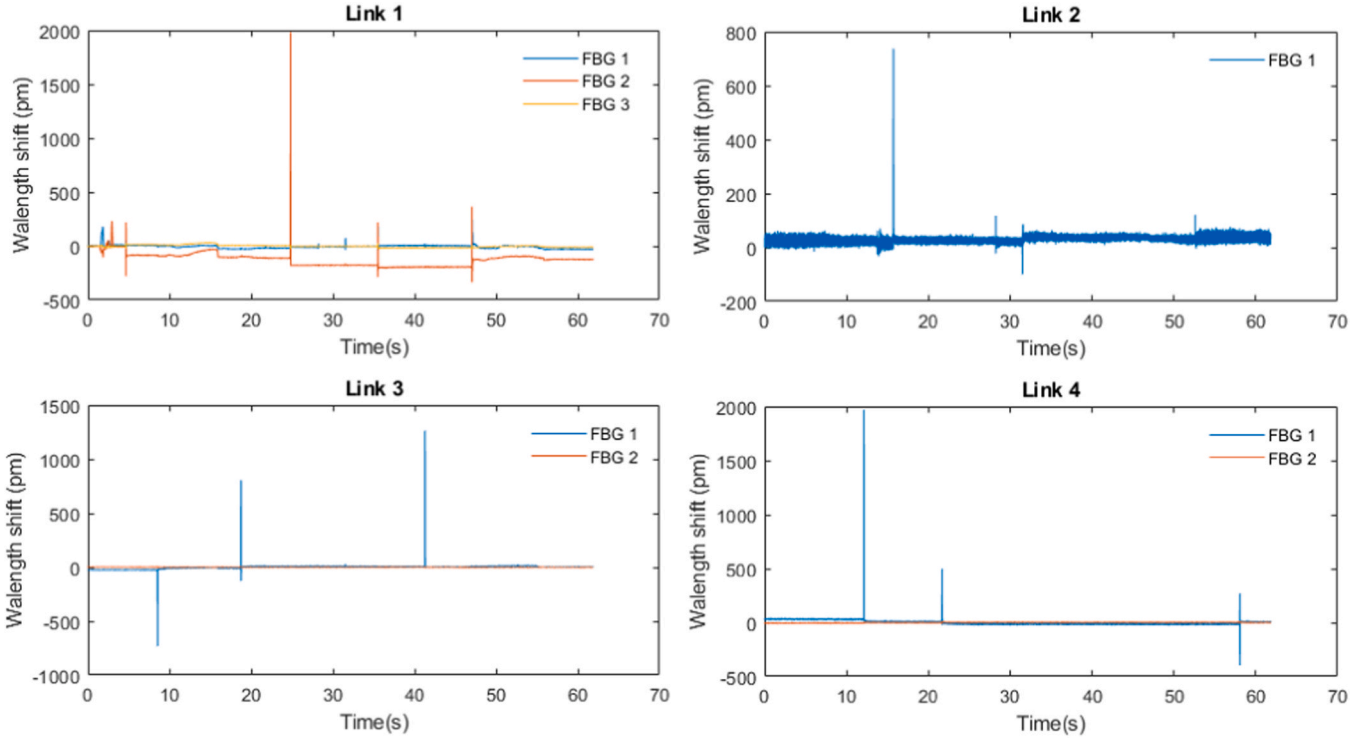

Fig. 12. Sensors response during the test with hits on the left side of the robot's body.

can be seen in Fig. 13. The spectrum signal of the optical fiber on link 2 presented high attenuation presumably due to the low quality of the used optical cables and this prevented the interrogator from detecting the peaks of the FBG 2. Then, FBG 1 was used in the procedure of impact detection for link 2.

From these results, the proposed tactile sensing system proved itself feasible to detect external interferences from the environment which can compromise the performance of the manipulator in service. Using the system, it is possible to detect the magnitude in terms of force, the instant of time and position on the robot body in which the impact

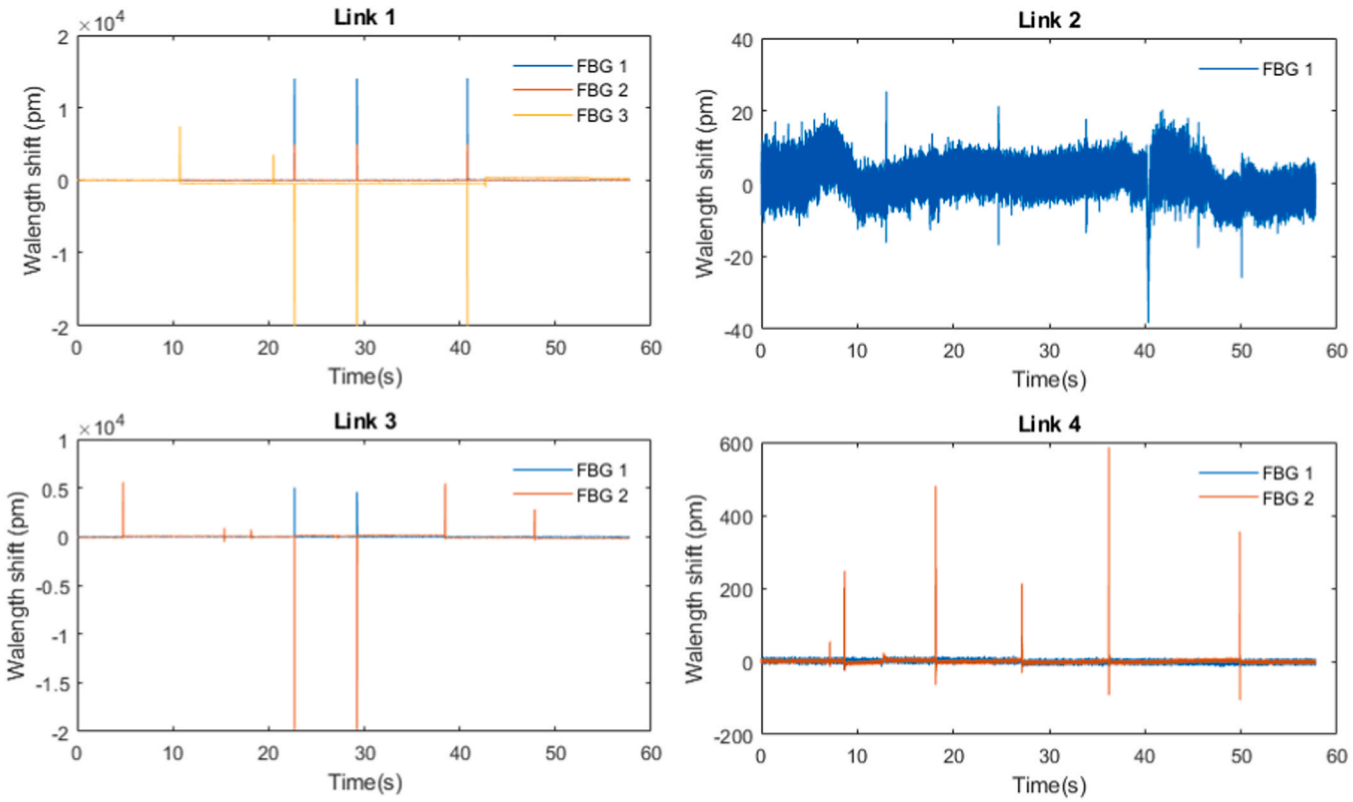

Fig. 13. Sensors response during the test with hits on the front side of the robot's body.

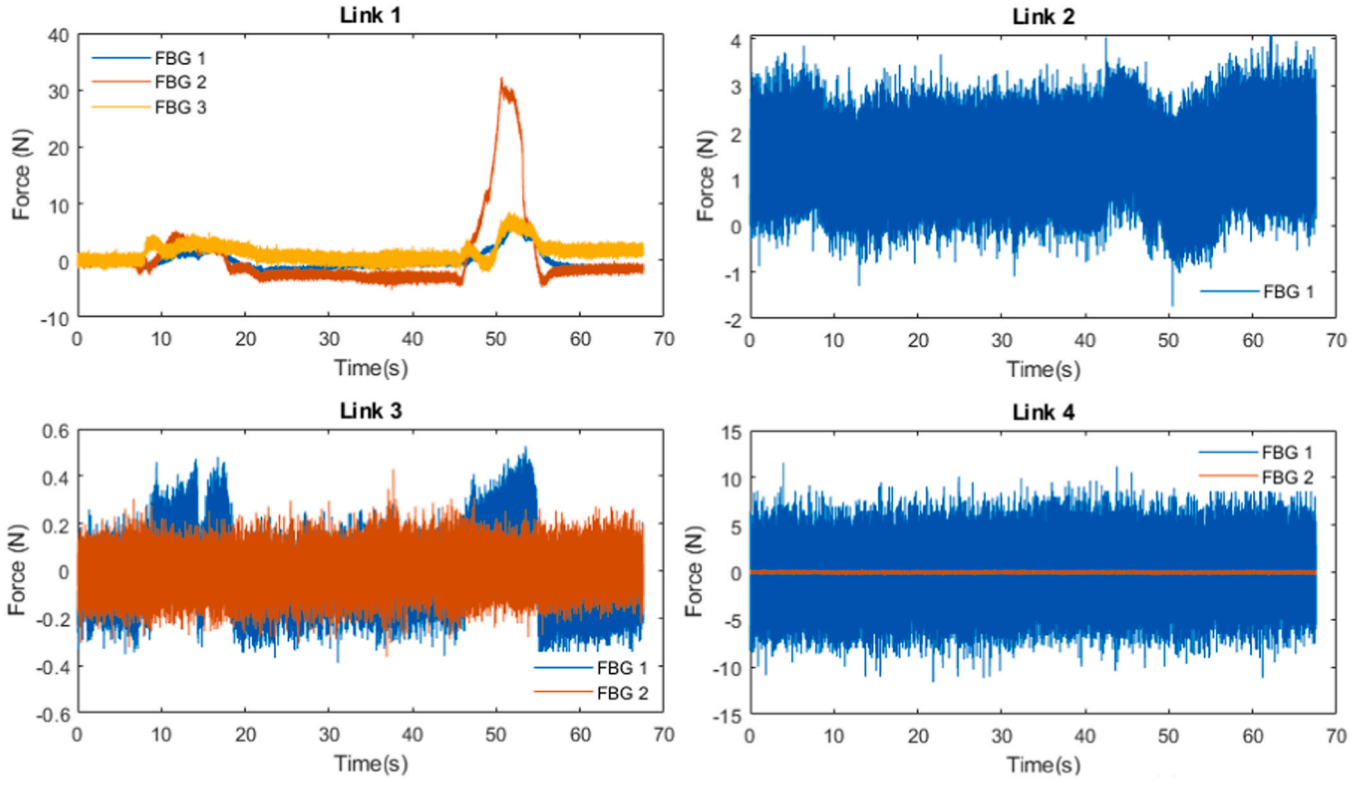

Fig. 14. Force response of each sensor during the test of the tactile system without external perturbations.

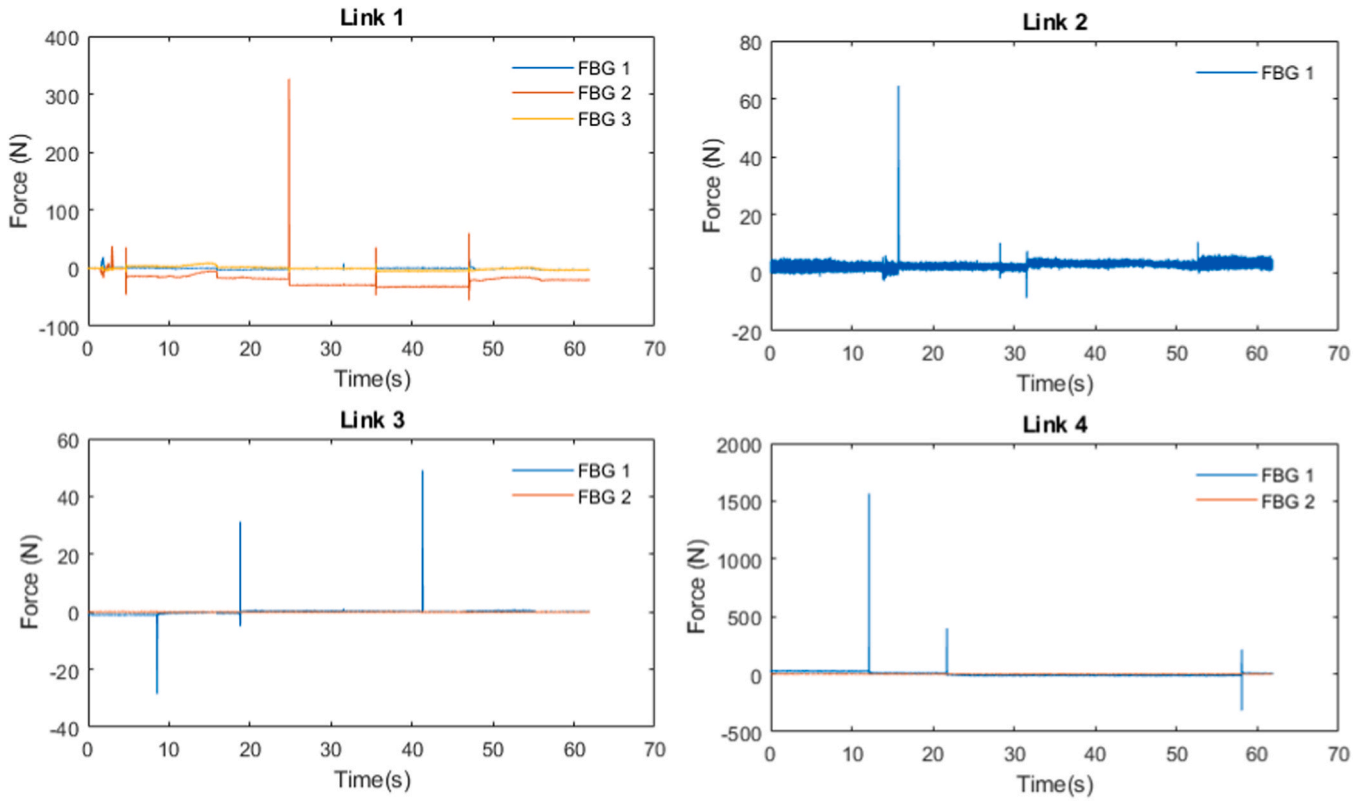

Fig. 15. Force response of each sensor during the test with hits on the left side of the robot's body.

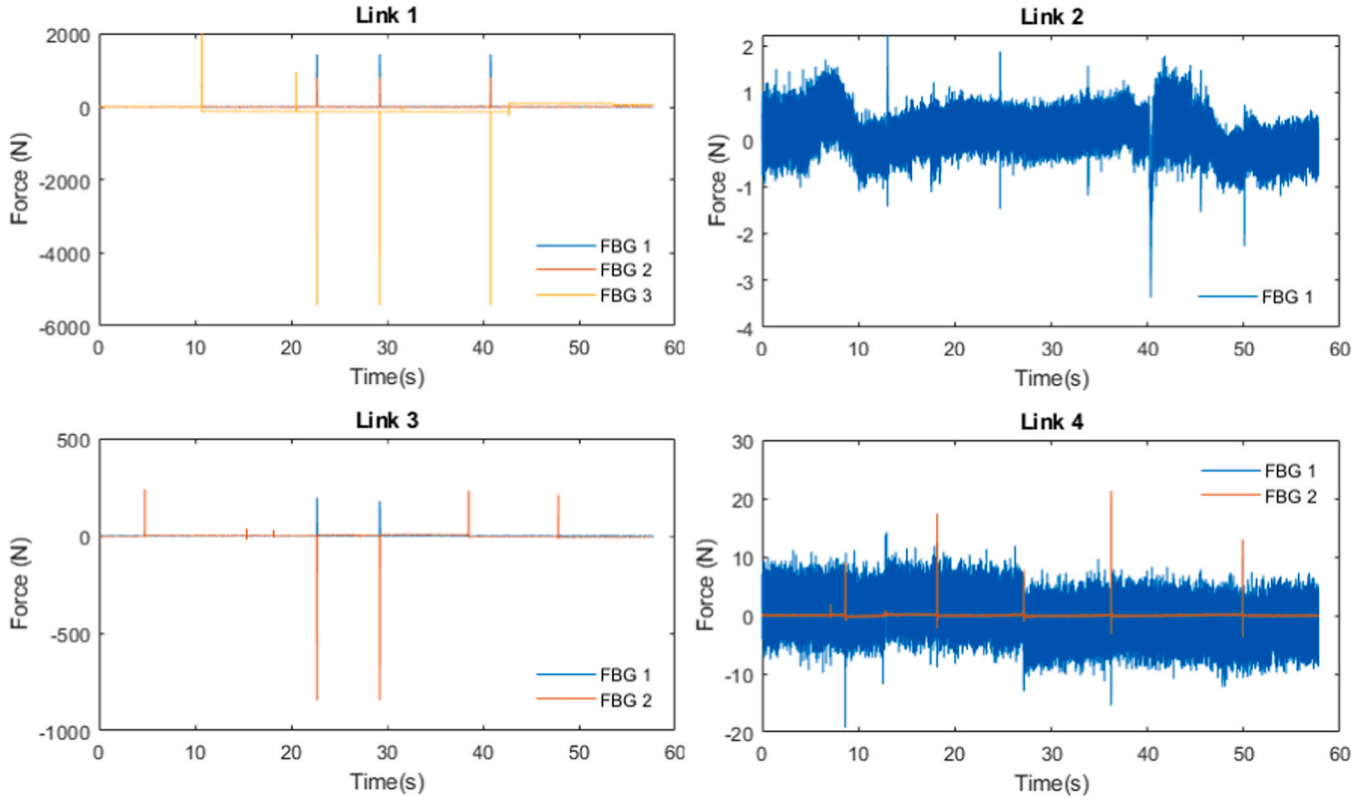

Fig. 16. Force response of each sensor during the test with hits on the front side of the robot's body.

happened. This system can be implemented together with an impedance control or other control strategy to make the industrial environment safer, especially in collaborative tasks with human beings. This is done by controlling the speed at which the robot must move and the times at which it must stop moving.

4. Conclusions

Human-robot interaction to perform a specific task ensures an environment in which the resource use effectiveness and productivity can be improved by combining robots' characteristics with flexibility and dexterity of humans in dealing with unexpected and non-repetitive tasks. Low-level control strategies alone are usually insufficient for the robot to develop group tasks with humans. For that reason, robots with amplified tactile sensitivity combined with modern control strategies make the work environment safer for human collaborators.

This paper proposed a FBG-based strategy to improve the tactile sensitivity of a robotic manipulator during operation. A mathematical model was proposed to estimate the distance of the sensors that guarantee the largest sensitive area for the system. After fabrication, the sensors were characterized in terms of force and temperature so that it is possible to implement a strategy to avoid cross-sensitivity effects.

The relation between force and temperature and Bragg wavelength shift showed a highly linear behavior (almost all R^2 superior to 0.94). As expected, the tactile system was not sensitive to the robot's movement and for this reason, complex processing algorithms were not necessary to separate the part of the signal related to external interference. From the results of the validation experiments, the system proved to be efficient in detecting the position and intensity of external impacts in real-time and to be a feasible alternative to work together with a performance improvement control system. For future works, it is suggested to use a portable multiplexing approach to extend the strategy to other types of robots, such as mobile or humanoid robots. Other suggestions are to use the FBGs to develop a robot digital twin system or to integrate the FBG based sensing systems into the robot control system to develop new collaborative control strategies.

CRediT authorship contribution statement

Conceptualization: V.B-N., A.G.L-J.; Methodology: V.B-N., A.G.L-J.; Formal analysis: V.B-N.; Funding acquisition: C.A.F.M., A.F-N., A.G.L-J.; Data analysis: V.B-N.; Validation: V.B-N.; Supervision: A.G.L-J.; Project administration: A.G.L-J.; Writing - Original Draft: V.B-N., C.A.F.M., A.F-N., A.G.L-J.; Writing - Review & Editing: V.B-N., C.A.F.M., A.F-N., A.G.L-J.

Declaration of Competing Interest

The authors declare that they have no known competing financial interests or personal relationships that could have appeared to influence the work reported in this paper.

Data Availability

Data will be made available on request.

Acknowledgements

This research is financed by FAPES (1004/2022 P: 2022–6PC5F, 458/2021, 2022-C5K3H), MCTI/FNDCT/FINEP 2784/20 and CNPq (304049/2019–0 and 310709/2021–0). The authors acknowledge financial support of the project i3N, UIDB/50025/2020 & UIDP/50025/2020, financed by national funds through the FCT/MEC. C. Marques thanks FCT through the CEECIND/00034/2018 (iFish project) and 2021.00667. CEECIND.

References

[1] P. Prisecaru, Challenges of the fourth industrial revolution, in: Knowledge Horizons. Economics, 8, Dimitrie Cantemir Christian University, 2016, p. 57.
[2] L. Romeo, et al., Internet of robotic things in smart domains: Applications and challenges, in: Sensors, 20, Multidisciplinary Digital Publishing Institute, 2020, p. 3355.
[3] M.A.K. Bahrin, et al., Industry 4.0: a review on industrial automation and robotic, J. Teknol. 78 (6–13) (2016).
[4] S. Vaidya, P. Ambad, S. Bhosle, Industry 4.0–a glimpse, in: Procedia manufacturing, 20, Elsevier, 2018, pp. 233–238.
[5] K.-D. Thoben, S. Wiesner, T. Wuest, "industrie 4.0" and smart manufacturing-a review of research issues and application examples, in: International journal of automation technology, 11, Fuji Technology Press Ltd., 2017, pp. 4–16.
[6] A.M. Okamura, M.J. Matarić, H.I. Christensen, Medical and health-care robotics, in: IEEE Robotics & Automation Magazine, 17, IEEE, 2010, pp. 26–37.
[7] R. Gassert, V. Dietz, Rehabilitation robots for the treatment of sensorimotor deficits: a neurophysiological perspective, J. Neuroeng. Rehabil. 15 (1) (2018) 1–15.
[8] A.M. Okamura, Haptic feedback in robot-assisted minimally invasive surgery, Curr. Opin. Urol. 19 (1) (2009) 102.
[9] A. Langer, et al., Trust in socially assistive robots: Considerations for use in rehabilitation, in: Neuroscience & Biobehavioral Reviews, 104, Elsevier, 2019, pp. 231–239.
[10] Y. She, et al., Exoskeleton-covered soft finger with vision-based proprioception and tactile sensing, IEEE. 2020 IEEE Int. Conf. Robot. Autom. (ICRA) (2020) 10075–10081.
[11] C.A. Diaz, et al., Optical fiber sensing for sub-millimeter liquid-level monitoring: a review, in: IEEE Sensors Journal, 19, IEEE, 2019, pp. 7179–7191.
[12] L. Yu, et al., Dual-core capacitive microfiber sensor for smart textile applications, in: ACS applied materials & interfaces, 11, ACS Publications, 2019, pp. 33347–33355.
[13] H.-E. Joe, et al., A review on optical fiber sensors for environmental monitoring, in: International journal of precision engineering and manufacturing-green technology, 5, Springer, 2018, pp. 173–191.
[14] A. Barrias, et al., Application of distributed optical fiber sensors for the health monitoring of two real structures in barcelona, in: Structure and Infrastructure Engineering, 14, Taylor & Francis, 2018, pp. 967–985.
[15] K. Peters, Polymer optical fiber sensors—a review, in: Smart materials and structures, 20, IOP Publishing, 2010.
[16] A.G. Leal-Junior, et al., Development of polymer optical fiber sensors for lower limb exoskeletons instrumentation. International Symposium on Wearable Robotics, SPRINGER, 2018, pp. 155–159.
[17] B.M. Quandt, et al., Body-monitoring and health supervision by means of optical fiber-based sensing systems in medical textiles. Advanced healthcare materials, Wiley Online Libr. 4 (3) (2015) 330–355.
[18] A. Leal-Junior, et al., Polymer optical fiber-based integrated instrumentation in a robot-assisted rehabilitation smart environment: A proof of concept, in: Sensors, 20, Multidisciplinary Digital Publishing Institute, 2020, p. 3199.
[19] A. Leal-Junior, et al., Smart textiles for multimodal wearable sensing using highly stretchable multiplexed optical fiber system, in: Scientific Reports, 10, Nature Publishing Group, 2020, pp. 1–12.
[20] Yong-Lae Park, et al., Force sensing robot fingers using embedded fiber Bragg grating sensors and shape deposition manufacturing. Proceedings 2007 IEEE International Conference on Robotics and Automation, IEEE, 2007, pp. 1510–1516.
[21] Hoseok Song, Kiyoung Kim, Jungju Lee, Development of optical fiber Bragg grating force-reflection sensor system of medical application for safe minimally invasive robotic surgery, Rev. Sci. Instrum. 82 (7) (2011), 074301.
[22] Pouya Soltani Zarrin, et al., Development of a 2-DOF sensorized surgical grasper for grasping and axial force measurements, IEEE Sens. J. 18 (7) (2018) 2816–2826.
[23] Berk Gonenc, et al., 3-DOF force-sensing motorized micro-forceps for robot-assisted vitreoretinal surgery, IEEE Sens. J. 17 (11) (2017) 3526–3541.
[24] L.K. Hillbrick, et al., Determination of the transverse modulus of cylindrical samples by compression between two parallel flat plates. *SN Applied Sciences*, Springer 1 (7) (2019) 1–11.
[25] Lundberg, G.; Yhland, E. Cylinder compressed between two plane bodies. [S.l.]: SKF, 1949.
[26] C.A. Díaz, et al., Liquid level measurement based on fbg-embedded diaphragms with temperature compensation, *IEEE Sens. J.*, IEEE 18 (1) (2017) 193–200.
[27] P. Wierzba, B. Kosmowski, Application of polarisation-maintaining side-hole fibres to direct force measurement, *Optoelectron. Rev.*, SIGMA NOT LTD (4) (2003) 305–312.
[28] R. Ackerley, et al., Touch perceptions across skin sites: differences between sensitivity, direction discrimination and pleasantness, *Front. Behav. Neurosci.*, Front. 8 (2014) 54.
[29] B.A. Tahir, et al., Effect of sensor gauge length on strain sensitivity of a fiber bragg grating system, Chin. J. Phys. 49 (5) (2011) 1035–1045.
[30] Rui Min, et al., Inscription of Bragg gratings in undoped PMMA mPOF with Nd: YAG laser at 266 nm wavelength, Opt. Express 27 (26) (2019) 38039–38048.
[31] Zhibin Li, Shuai Li, Xin Luo, An overview of calibration technology of industrial robots, IEEE/CAA J. Autom. Sin. 8 (1) (2021) 23–36.
[32] Singh, Puneet Kumar, Krishna, C. Murali, Continuum arm robotic manipulator: a review, Univers. J. Mech. Eng. 2 (6) (2014) 193–198.
[33] Andreas Antoniou, Digit. Signal Process.: Signals, Syst., Filters (2005).

[34] Mengying Tan, et al., A temperature-compensated fiber Bragg grating sensor system based on digital filtering for monitoring the pantograph–catenary contact force, Proc. Inst. Mech. Eng., Part F: J. Rail Rapid Transit 233 (2) (2019) 187–200.
[35] Michael A. Babyak, What you see may not be what you get: a brief, nontechnical introduction to overfitting in regression-type models, Psychosom. Med. 66 (3) (2004) 411–421.
[36] Arnaldo Gomes Leal-Junior, Anselmo Frizera, Maria José Pontes, Dynamic compensation technique for POF curvature sensors, J. Light. Technol. 36 (4) (2018) 1112–1117.
[37] Arnaldo G. Leal-Junior, et al., Viscoelastic features based compensation technique for polymer optical fiber curvature sensors, Opt. Laser Technol. 105 (2018) 35–40.
[38] Arnaldo Gomes Leal-Junior, et al., Hysteresis compensation technique applied to polymer optical fiber curvature sensor for lower limb exoskeletons, Meas. Sci. Technol. 28 (12) (2017), 125103.
[39] Arnaldo G. Leal-Junior, et al., Polymer optical fiber sensors in wearable devices: toward novel instrumentation approaches for gait assistance devices, IEEE Sens. J. 18 (17) (2018) 7085–7092.

Vitorino Biazi-Neto is a Ph.D. student with the Department of Physics, University of Aveiro, Portugal. He received the B.S. degree in mechanical engineering and the M.S. degree in electrical engineering from the Federal University of Espírito Santo in 2019 and 2022, respectively. His main research interests are instrumentation, robotic systems and sensors.

Carlos A. F. Marques received the Ph.D. degree in physics engineering from the University of Aveiro, Aveiro, Portugal, in 2013. He was a Marie Curie (MC) Fellow of the Aston Institute of Photonics Technologies, Aston University, Birmingham, U.K., until March 2016. He is currently a Research Scientist with the Department of Physics and the Institute of Nanostructures, Nanomodelling and Nanofabrication (I3N), University of Aveiro. His main research interests include optical devices for sensing, integrated optics, low-cost interrogation systems, machine learning, data acquisition, and optical transmission data.

Anselmo Frizera-Neto received the B.S. degree in electrical engineering from the Federal University of Espirito Santo (UFES), Vitória, Brazil, in 2006, and the Ph.D. degree in electronics from the Universidad de Alcalá, Spain, in 2010. From 2006–2010, he was a Researcher with the Bioengineering Group, Spanish National Research Council (CSIC). He is currently a Professor at the Department of Electrical Engineering, UFES. His research interests include rehabilitation robotics, human–machine interaction, and movement analysis.

Arnaldo G. Leal-Junior received the B.S. degree in mechanical engineering and the Ph.D. degree in electrical engineering from the Federal University of Espírito Santo in 2015 and 2018, respectively. He currently is a Professor with the Department of Mechanical Engineering, Federal University of Espírito Santo, Vitoria, Brazil. His research interests include optical fiber sensors with an emphasis on polymer optical fiber sensors, robotic systems, instrumentation, and actuators.